

# Calculation of thermal neutron albedo for mono-material and bi-material reflectors

Sara Azimkhani<sup>1</sup> · Farhad Zolfagharpour<sup>1</sup> · Farhood Ziaie<sup>2</sup>

Received: 29 September 2017 / Revised: 23 March 2018 / Accepted: 27 March 2018 / Published online: 27 July 2018

© Shanghai Institute of Applied Physics, Chinese Academy of Sciences, Chinese Nuclear Society, Science Press China and Springer Nature Singapore Pte Ltd. 2018

**Abstract** Thermal neutron albedo has been investigated for different thicknesses of mono-material and bi-material reflectors. An equation has been obtained for a bi-material reflector by considering the neutron diffusion equation. The bi-material reflector consists of binary combinations of water, graphite, lead, and polyethylene. An experimental measurement of thermal neutron albedo has also been conducted for mono-material and bi-material reflectors by using a  $^{241}\text{Am}$ –Be (5.2 Ci) neutron source and a  $\text{BF}_3$  detector. The maximum value of thermal neutron albedo was obtained for a polyethylene–water combination ( $0.95 \pm 0.02$ ).

**Keywords** Neutron current · Bi-material reflector · Thermal neutron albedo ·  $\text{BF}_3$  detector · Reflection · Diffusion equation

## 1 Introduction

The efficiency of a neutron reflector is calculated using the neutron reflection coefficient or neutron albedo. The neutron albedo is the ratio of neutrons reflected back into the reactor to the number of neutrons entering the reflector. Neutron albedo values have been extensively used for

measuring neutron reflector effectiveness, analysis of bulk samples, neutron dosimetry, neutron shielding, imaging and detection of explosive materials, and land mines [1–4]. The reflector efficiency is increased by increasing the scattering cross section and decreasing the absorption cross section of the reflector [5, 6]. Furthermore, the neutron reflection coefficient depends on the elemental composition of the reflector substance and the geometrical circumstances of the measurement [1]. Other researchers have studied neutron albedo values for different reflector types [3, 7]. Thermal neutron albedo measurements have been carried out for monolithic and geometry-voided reflectors [8]. The albedo calculation has also been produced for monoenergetic fast neutrons incidented on a variety of materials, and a neutron albedo approximation for intermediate energy neutrons (0.5 eV–0.2 MeV) has been proposed [9–11]. Formulas have been proposed for calculating thermal neutron albedo [3]. However, few studies have been performed for the thermal neutron albedo of reflectors containing two materials. In this work, the thermal neutron albedo was calculated for different thicknesses of four mono-material reflectors, and saturation thicknesses were obtained for each material. The materials used for mono-material reflectors were water, graphite, lead, and polyethylene. In order to increase the thermal neutron albedo, different thicknesses of the second material were added to the first material. The thermal neutron albedo equation for a bi-material reflector was obtained by using the neutron diffusion equation. The thermal neutron albedo for mono-material and bi-material reflectors was also measured using a setup that consisted of a 5.2 Ci neutron source,  $\text{BF}_3$  neutron detector, cadmium as neutron absorber, and water as neutron moderator.

✉ Sara Azimkhani  
sara.azimkhani@gmail.com

<sup>1</sup> Department of Physics, University of Mohaghegh Ardabili, P.O. Box 179, Ardabil, Iran

<sup>2</sup> Radiation Application Research School, Nuclear Science & Technology Research Institute, P.O. Box 11365-3486, Tehran, Iran

## 2 Theoretical aspects

### 2.1 Albedo of a mono-material reflector

The neutron albedo of a reflector is defined as a ratio of neutron currents exiting the reflector ( $J_{out}$ ) to neutron currents entering the reflector ( $J_{in}$ )

$$\beta = \frac{J_{out}}{J_{in}}. \tag{1}$$

The neutron albedo of an infinite plate is expressed as [12]

$$\beta = \frac{1 - \frac{2D}{L} \coth\left(\frac{a}{L}\right)}{1 + \frac{2D}{L} \coth\left(\frac{a}{L}\right)}, \tag{2}$$

where  $a$  is the thickness of the plate, and  $D$  and  $L$  are the diffusion coefficient and diffusion length, respectively, which are given by:

$$D = \frac{\Sigma_s}{3\Sigma_t^2}, \tag{3}$$

$$L = \sqrt{\frac{D}{\Sigma_a}}, \tag{4}$$

and  $\Sigma_s$ ,  $\Sigma_t$ , and  $\Sigma_a$  are the macroscopic scattering cross section, total cross section, and absorption cross section of reflector, respectively.

Thermal neutron cross sections were derived from Lamarsh [13] and Sears [14] for calculation of the thermal neutron albedo using Eq. (2). Then,  $D$  and  $L$  were calculated according to Eqs. (3) and (4) for water, graphite, lead, and polyethylene as mono-material reflectors. Equation (2) was used for an infinite plate along the  $y$ - and  $z$ -axis and placed between planes  $x = 0$  and  $x = a$ . The neutron flux was assumed to be zero at  $x = a$ ; therefore, the curve of the thermal neutron albedo was saturated with steep slope at low thicknesses. However, in practice, the reflector dimension is a finite plate that goes to zero at  $x = a$ . Thus, we enter  $F\left(\frac{a}{L}\right)$  as the corrected function to improve Eq. (2).

$$\beta = \frac{1 - \frac{2D}{L} F\left(\frac{a}{L}\right) \coth\left(\frac{a}{L}\right)}{1 + \frac{2D}{L} F\left(\frac{a}{L}\right) \coth\left(\frac{a}{L}\right)}, \tag{5}$$

where

$$F\left(\frac{a}{L}\right) = a_1 e^{-a_2 \frac{a}{L}} + a_3. \tag{6}$$

The  $F\left(\frac{a}{L}\right)$  function causes that the slope of thermal neutron albedo curve to become less steep. The values of  $a_1$ ,  $a_2$ , and  $a_3$  were calculated for the materials used via fitting the experimental data.

### 2.2 Albedo of a bi-material reflector

The neutron albedo of two infinite plates with two different materials was calculated by the diffusion equation. The first reflector was located between  $x = 0$  and  $x = a$ , and the second reflector was located between  $x = a$  and  $x = b$ . The neutrons have been assumed to enter via the face  $x = 0$  uniformly; therefore, the flux is only dependent on  $x$ , and there are no sources within the reflector. The diffusion equation could be defined as:

$$\frac{d^2 \Phi(x)}{dx^2} - \frac{1}{L} \Phi(x) = 0. \tag{7}$$

The neutron fluxes of two reflectors are expressed according to  $\Phi_1(x)$  and  $\Phi_2(x)$

$$\Phi_1(x) = A_1 \sinh\left(\frac{x}{L_1}\right) + A_2 \cosh\left(\frac{x}{L_1}\right), \tag{8}$$

$$\Phi_2(x) = A_3 \sinh\left(\frac{b-x}{L_2}\right), \tag{9}$$

where the neutron fluxes remain finite as  $x \rightarrow \infty$ . Since both the neutron fluxes and the neutron currents remain continuous across the interfaces (as  $x = a$ ), it can be assumed that:

$$\Phi_1(x)|_{x=a} = \Phi_2(x)|_{x=a}, \tag{10}$$

$$D_1 \frac{d\Phi_1(x)}{dx} \Big|_{x=a} = D_2 \frac{d\Phi_2(x)}{dx} \Big|_{x=a}. \tag{11}$$

Therefore, the constants  $A_1$ ,  $A_2$ , and  $A_3$  in the flux equations can be calculated using Eqs. (10) and (11) as:

$$\frac{A_1}{A_2} = - \frac{D_1 L_2 \sinh\left(\frac{-b+a}{L_2}\right) \sinh\left(\frac{a}{L_1}\right) - D_2 L_1 \cosh\left(\frac{-b+a}{L_2}\right) \cosh\left(\frac{a}{L_1}\right)}{D_1 L_2 \sinh\left(\frac{-b+a}{L_2}\right) \cosh\left(\frac{a}{L_1}\right) - D_2 L_1 \cosh\left(\frac{-b+a}{L_2}\right) \sinh\left(\frac{a}{L_1}\right)}, \tag{12}$$

$$\frac{A_1}{A_3} = - \frac{D_1 L_2 \sinh\left(\frac{-b+a}{L_2}\right) \sinh\left(\frac{a}{L_1}\right) - D_2 L_1 \cosh\left(\frac{-b+a}{L_2}\right) \cosh\left(\frac{a}{L_1}\right)}{D_1 L_2 \left(\sinh^2\left(\frac{a}{L_1}\right) - \cosh^2\left(\frac{a}{L_1}\right)\right)}, \tag{13}$$

where  $D$  and  $L$  are the diffusion coefficient and diffusion length, respectively, for the first and the second reflectors according to the defined indices. Thus,  $J_{in}$  and  $J_{out}$  are derived from the diffusion equation as:

$$J_{in} = \frac{\Phi_1}{4} - \frac{D_1}{2} \frac{\partial \Phi_1}{\partial x} \Big|_{x=0} = \frac{A_2}{4} - \frac{D_1 A_1}{2L_1}, \tag{14}$$

$$J_{out} = \frac{\Phi_1}{4} + \frac{D_1}{2} \frac{\partial \Phi_1}{\partial x} \Big|_{x=0} = \frac{A_2}{4} + \frac{D_1 A_1}{2L_1}. \tag{15}$$

Therefore, the neutron albedo for a bi-material reflector yields the following equation:

$$\beta_2 = \frac{j_{out}}{j_{in}} = \frac{1 + \frac{2D_1 A_1}{L_1 A_2}}{1 - \frac{2D_1 A_1}{L_1 A_2}} \tag{16}$$

The thermal neutron albedo is obtained from Eq. (16) for a bi-material reflector. Similar to the corrected thermal neutron albedo equation for a mono-material reflector, Eq. (16), is improved by the function  $G(\frac{b}{L})$ :

$$\beta_2 = \frac{j_{out}}{j_{in}} = \frac{1 + \frac{2D_1}{L_1} G(\frac{b}{L}) \frac{A_1}{A_2}}{1 - \frac{2D_1}{L_1} G(\frac{b}{L}) \frac{A_1}{A_2}}, \tag{17}$$

where

$$G\left(\frac{b}{L}\right) = b_1 e^{-b_2 \frac{b}{L}} + b_3, \tag{18}$$

where the  $b_1$ ,  $b_2$ , and  $b_3$  coefficients in Eq. (18) were obtained via fitting the experimental data of the thermal neutron albedo.

### 2.3 Decline rate of reflector in high flux reactor

Flux can be considerably affected by the absorption of neutrons in a high flux reactor and therefore the absorption cross section of an ideal reflector should be small and the decline rate of a reflector should be calculated. In ordinary flux, the decline value of a reflector is negligible. The thermal flux density is approximately  $10^{15}$  neutrons/cm<sup>2</sup> s<sup>-1</sup> in the high flux reactor [15]. The interaction rate per unit volume of a reflector is obtained using the equation below [13]:

$$\text{Interaction rate} = \sigma In, \tag{19}$$

where  $\sigma$ ,  $I$ , and  $n$  are the neutron microscopic absorption cross section, the number of neutrons that strike the reflector per cm<sup>2</sup> s<sup>-1</sup>, and the total number of atoms per unit volume of a reflector, respectively. Therefore, the decline value of a reflector per unit time with a given volume of the reflector is defined as:

$$\frac{1}{n} \frac{dN_R}{dt} = \sigma I, \tag{20}$$

where  $N_R$  is the decline value of reflector when a supposed reactor works in the range of time  $t_i$ . The decline percentage of a reflector per unit volume of the reflector is expressed as:

$$\text{Decline percentage} = \int_0^{t_i} 100 \frac{1}{n} \frac{dN_R}{dt} dt = 100 \sigma I t_i. \tag{21}$$

### 3 Experimental procedures

A 5.2 Ci <sup>241</sup>Am–Be source was located in a container filled with water 10 cm away from one of the container walls. Water, as fast neutron moderator, can produce thermal neutron current. A BF<sub>3</sub> detector (2.5 cm in diameter and 20 cm in length) was placed at 14 cm distance from the neutron source. In order to prevent the direct interaction of thermal neutrons with the detector, a cadmium sheet with dimension 23 cm × 31 cm × 0.4 cm was placed between the source and the detector. Thus, only the thermal neutron current reflecting through the reflector could be detected ( $J_{out}$ ). The thermal neutron current ( $J_{in}$ ) entering the reflector could be detected by replacing the BF<sub>3</sub> detector as well as the reflector. In this experiment, water, graphite, polyethylene, and lead in both monolithic and multilithic forms were used as the materials for thermal neutron reflectors with different thicknesses (20 cm in width and 30 cm in length). A multichannel analyzer (MCA) and NTMCA software were used for data analysis. The measuring instrument is shown in Fig. 1.

### 4 Results and discussion

The theoretical and experimental results of thermal neutron albedo measurements are shown in Fig. 2 as a function of reflector thickness with line and scatter curves, respectively. The thermal neutron albedo of the mono-material reflectors was obtained using Eqs. (1) and (5). The values of  $a_1$ ,  $a_2$ , and  $a_3$  are shown in Table 1. Also,  $J_{in}$  and  $J_{out}$  were measured using the BF<sub>3</sub> detector for different thicknesses of water, graphite, lead, and polyethylene



Fig. 1 (Color online) Photograph of experimental setup

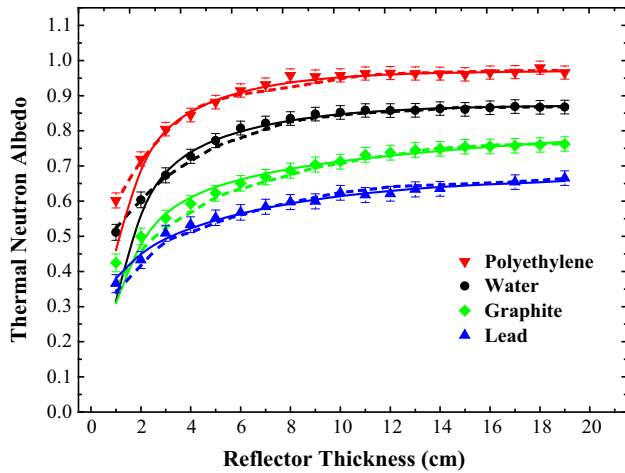


**Fig. 2** (Color online) Thermal neutron albedo as a function of reflector thickness for water, graphite, lead, and polyethylene mono-material reflectors. Theoretical results extracted from Eq. (5) and experimental results are shown with line and scatter curves, respectively. Also, simulated results using MCNPX code are shown with a short dashed curve

**Table 1** Coefficients of Eq. (6) for mono-material reflectors

Material	$a_1$	$a_2$	$a_3$
Water	2.3449	0.5564	0.7363
Graphite	- 1.9347	2.7155	2.1458
Lead	- 1.3703	1.9580	1.4306
Polyethylene	2.2273	0.5363	0.1657

reflectors. Furthermore, the experimental geometry was designed using MCNPX code, and simulation results were compared with experimental and theoretical results.

According to Fig. 2, thermal neutron albedo increases with reflector thickness before reaching saturation at what is called the “saturation thickness.” Saturation thickness is 7, 16, 10, and 8 cm for water, graphite, lead, and polyethylene reflectors, respectively. The maximum observed value of thermal neutron albedo was for polyethylene due to its high hydrogen content. Water, graphite, and lead reflectors had lower subsequent values of thermal neutron albedo, respectively. Under identical geometric conditions, thermal neutron reflection depends on the hydrogenous components and atomic number of reflector materials. Therefore, thermal neutrons albedo reaches a maximum for the polyethylene reflector. However, water is used more than polyethylene as a neutron reflector for thermal reactors because of safety aspects. Lead reflectors are also used for fast reactors because of the low neutron spectral shift [10]. The thermal neutron albedo for binary combinations of reflectors is shown in Figs. 3, 4, 5 and 6 as a function of

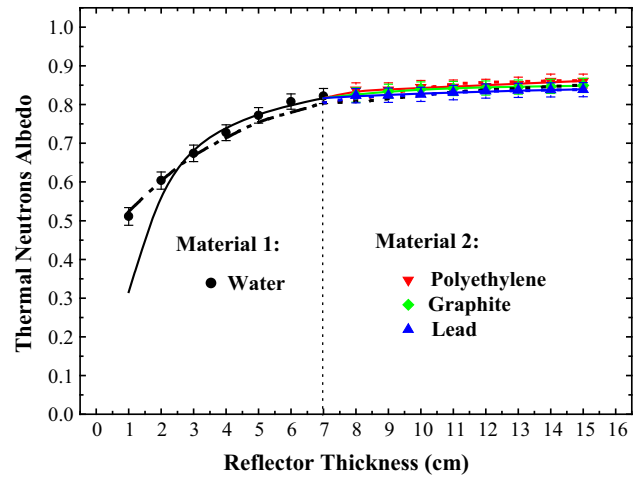


**Fig. 3** (Color online) The thermal neutron albedo for water–polyethylene, water–graphite, and water–lead combinations. Theoretical results extracted from Eq. (17) and experimental results are shown with line and scatter curves, respectively. Also, simulated results by using MCNPX code are shown with short dashed curve

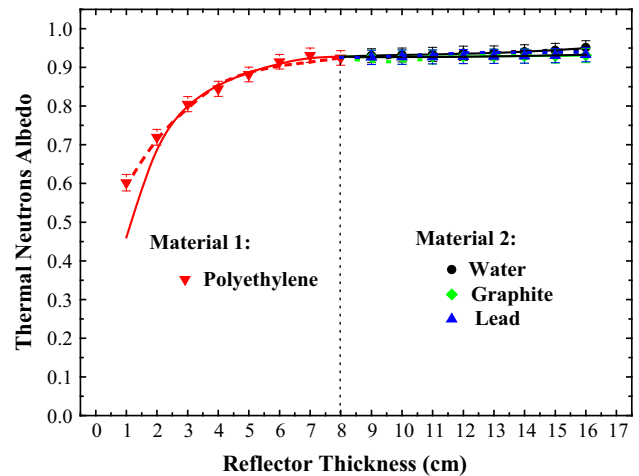


**Fig. 4** (Color online) The thermal neutron albedo for polyethylene–water, polyethylene–graphite, and polyethylene–lead combinations. Theoretical results extracted from Eq. (17) and experimental results are shown with line and scatter curves, respectively. Also, simulated results by using MCNPX code are shown with short dashed curve

reflector thickness. The values of  $b_1$ ,  $b_2$ , and  $b_3$  are shown in Table 2. The first material is fixed at saturation thickness, and the second material with different thicknesses is added to the first reflector. Thermal neutrons are reflected from two successive diffusing districts in the bi-material reflector.

According to Figs. 3, 4, 5 and 6, the thermal neutron albedo is increased by adding the second material with the condition that the reflection coefficient for the first material is lower than the reflection coefficient for the second material. In this circumstance, neutron currents exiting the reflector ( $J_{out}$ ) are increased and so the thermal neutron

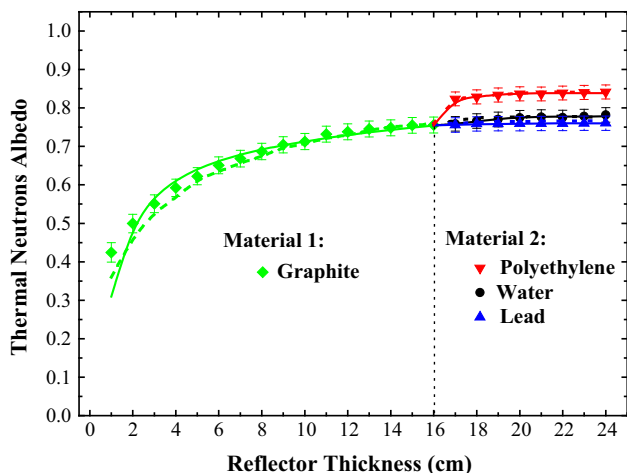


**Fig. 5** (Color online) The thermal neutron albedo for graphite–polyethylene, graphite–water, and graphite–lead combinations. Theoretical results extracted from Eq. (17) and experimental results are shown with line and scatter curves, respectively. Also, simulated results by using MCNPX code are shown with short dashed curve

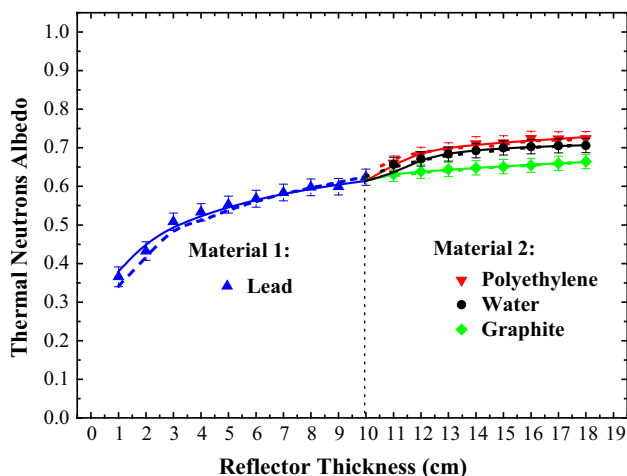


**Fig. 6** (Color online) The thermal neutron albedo for lead–polyethylene, lead–water, and lead–graphite combinations. Theoretical results extracted from Eq. (17) and experimental results are shown with line and scatter curves, respectively. Also, simulated results by using MCNPX code are shown with short dashed curve

albedo is raised in the bi-material reflector. Adding a polyethylene reflector to water, graphite, or lead materials slightly increases the thermal neutron albedo because the albedo coefficient of the polyethylene reflector is higher than those of the other materials used as thermal neutron reflectors. Also, the thermal neutron albedo does not increase in the binary combinations of water–graphite, water–lead, or graphite–lead. In these combinations, the second materials have lower neutron reflection properties than the first materials. However, the thermal neutron albedo increases in bi-material reflectors of water–polyethylene (4.65%), graphite–polyethylene (10.71%),

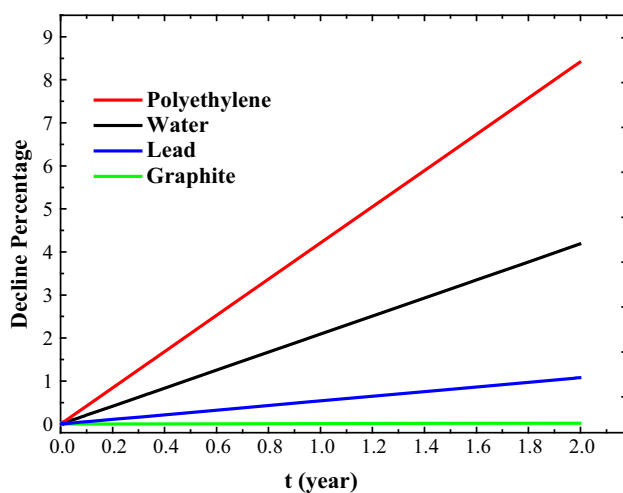
graphite–water (3.84%), lead–polyethylene (13.89%), lead–graphite (6.06%), and lead–water (11.42%).

Thermal neutron absorption cross sections are related to the  $(n, \gamma)$  reaction in water, graphite, lead, and polyethylene reflectors. However, there is the  $(n, n + A)$  reaction for lead reflectors, which is negligible ( $10^{-20}$  barn). Cross sections of natural isotopes of lead, carbon, oxygen, and hydrogen were extracted from the Evaluated Nuclear Data File [16]. Then, decline percentages of reflectors were obtained for the high fluxes according to Eq. (21). The decline percentages per unit volume for the reflectors are shown in Fig. 7 as a function of time. The basic materials of reflectors are reduced, and the absorption reaction products are increased such that these variations are proportional to the decline percentage of reflectors. Therefore, the cross sections of reflectors and, consequently, the neutron albedo are changed. Cross sections of the  $(n, \gamma)$  reaction products were also extracted from the Evaluated Nuclear Data File for water, graphite, lead, and polyethylene reflectors [16]. Then, the neutron albedo coefficients were calculated [Eq. (5)] by considering the decline values and the variation of reflector cross sections. The variation in the percentage of neutron albedo for polyethylene, water, graphite, and lead reflectors is shown in Table 3.

According to Fig. 7, the decline values of water, graphite, lead, and polyethylene reflectors increase over time. Graphite has a low-absorption cross section for thermal neutrons (0.0035 barn), and its decline value was constant. The absorption cross section for thermal neutrons is 0.171 barn for the lead reflector, so the variation of decline value was low. Polyethylene and water reflectors had somewhat high variation of decline values, because thermal neutrons have an absorption cross section of 0.3320 barn for hydrogen. The thermal neutron albedo coefficients in high flux reactor are changed slightly for water, graphite, lead, and polyethylene reflectors. These values are negligible even after 2 years, as shown in Table 3. Therefore, the thermal neutron reflection coefficients are not changed in the high flux reactors. Previous works have reported an experimentally derived thermal neutron albedo equal to  $0.80 \pm 0.024$  for water [8]. Also, albedo coefficients have been obtained as 0.80 and 0.94 for water and graphite reflectors, respectively [12]. These values are for the saturation thicknesses and have been calculated using neutron diffusion theory. We have found that these values agree with our results. It is worth noting that thermal neutron albedo has not been investigated previously for the binary combinations we used. There is also reasonable agreement between the theoretical and experimental values, and the simulation results are derived using MCNPX code.

**Table 2** Coefficients of Eq. (18) for bi-material reflectors

Material	$b_1$	$b_2$	$b_3$
Water-graphite	4.0672	0.8540	0.8835
Water-polyethylene	2.1547E4	2.1895E-6	- 2.1545E4
Water-lead	0.5045	0.2115	0.8360
Graphite-water	- 3.2140	2.5575	2.8016
Graphite-polyethylene	- 2.3922E13	1.0731E2	1.5899
Graphite-lead	1.8267	2.4817	1.2907
Lead-water	1.8267	2.4817	1.2907
Lead-polyethylene	1.09116	0.8543	0.9168
Lead-graphite	- 1.4427	1.8427	1.4315
Polyethylene-water	- 0.0015	- 0.4781	0.4076
Polyethylene-graphite	- 0.0273	- 0.1094	4.6663
Polyethylene-lead	- 4.3940E-4	- 0.4937	0.4227

**Fig. 7** (Color online) The decline percentage of water, graphite, lead, and polyethylene reflectors versus time in the high flux reactor**Table 3** Albedo variation and decline percentages in high flux reactors after 2 years for mono-material reflectors

Material	Decline percentage	Albedo variation percentage
Water	4.1832	0.0460
Graphite	0.0220	0.0013
Lead	1.0773	0.2623
Polyethylene	8.4105	0.1812

## 5 Conclusion

Reasonable agreements were found between the theoretical and the experimental results of thermal neutron albedo calculated using the selected functions for mono-material and bi-material reflectors. The obtained thermal neutron albedo values were  $0.86 \pm 0.02$  for water-polyethylene,  $0.84 \pm 0.02$  for graphite-polyethylene,

$0.95 \pm 0.02$  for polyethylene-water, and  $0.66 \pm 0.02$  for lead-graphite combinations. The results show that thermal neutron albedo depends on the material type and thickness of reflectors. Additionally, when the thermal neutron reflection coefficient of the first layer of a reflector is lower than that of the second layer, the thermal neutron albedo increases with added thickness of the second layer. Finally, use of bi-material reflectors could be effective for neutron shielding. If lead is used as one of the materials in bi-material reflectors, it could also shield against gamma rays.

## References

1. J. Csikai, C.M. Buczko, The concept of the reflection cross section of thermal neutrons. *Appl. Radiat. Isot.* **50**, 487–490 (1999). [https://doi.org/10.1016/S0969-8043\(98\)00077-3](https://doi.org/10.1016/S0969-8043(98)00077-3)
2. V.D. Kovaltchouk, H.R. Andrews, E.T.H. Clifford et al., A neutron Albedo system with time rejection for landmine and IED detection. *Nucl. Instrum. Methods A* **652**, 84–89 (2011). <https://doi.org/10.1016/j.nima.2010.09.038>
3. S.M. Mirza, M. Tufail, M.R. Liaqat, Thermal neutron albedo and diffusion parameter measurements for monolithic and geometric voided reflectors. *Radiat. Meas.* **41**, 89–94 (2006). <https://doi.org/10.1016/j.radmeas.2005.03.005>
4. X. Li, Y. Wang, C. Huang et al., Design and simulation of time-of-flight neutron reflectometer. *Nucl. Sci. Tech.* **21**, 157–160 (2010). <https://doi.org/10.13538/j.1001-8042/nst.21.157-160>
5. S. Dawahra, K. Khattab, G. Saba, Study the effects of different reflector types on the neutronic parameters of the 10 MW MTR reactor using the MCNP4C code. *Ann. Nucl. Energy* **85**, 1115–1118 (2015). <https://doi.org/10.1016/j.anucene.2015.07.029>
6. B. Han, Y. Kim, C.H. Kim, Optimal configuration of neutron reflector in He-cooled molten Li blanket. *Fusion Eng. Des.* **81**, 729–732 (2006). <https://doi.org/10.1016/j.fusengdes.2005.05.008>
7. D.G. Cacuci, *Handbook of Nuclear Engineering. Volume 2: Reactor Design* (Springer, Berlin, 2010)
8. E.H.K. Akaho, S.A. Jonah, C.P.K. Dagadu et al., Geometrical effects on thermal neutron reflection of hydrogenous moderators using  $^{241}\text{Am}$ -Be source. *Appl. Radiat. Isot.* **55**, 175–179 (2001). [https://doi.org/10.1016/S0969-8043\(00\)00386-9](https://doi.org/10.1016/S0969-8043(00)00386-9)

9. R.C. Brockhoff, J.K. Shuitis, A new approximation for the neutron albedo. *Nucl. Sci. Eng.* **155**, 1–17 (2007). <https://doi.org/10.13182/NSE07-A2641>
10. S. Azimkhani, F. Zolfagharpour, F. Ziaie, Investigation of reflection properties of applied reflectors for thermal neutrons by considering the albedo and spectral shift. *Prog. Nucl. Energy* **100**, 192–196 (2017). <https://doi.org/10.1016/j.pnucene.2017.06.011>
11. B. Zhong, T.J. Liang, H. Zha et al., Neutronics analysis of the target-moderator-reflector (TMR) configuration for compact long pulsed neutron sources. *Nucl. Eng. Des.* **241**, 4720–4725 (2011). <https://doi.org/10.1016/j.nucengdes.2011.02.032>
12. P. Reuss, *Neutron Physics* (EDP Sciences, Les Ulis, 2008)
13. J.R. Lamarsh, A.G. Barata, *Introduction to Nuclear Engineering*, 3rd edn. (Prentice Hall, Inc., New Jersey, 2001)
14. V.F. Sears, Neutron scattering lengths and cross section. *Neutron News* **3**, 26–37 (1992). <https://doi.org/10.1080/10448639208218770>
15. A. Vertes, S. Nagy, Z. Klencsar, R.G. Lovas, F. Rosch, *Handbook of Nuclear Chemistry*, 2nd edn. (Springer, Berlin, 2011)
16. ENDF, Evaluated Nuclear Data File. A computer file of evaluated experimental nuclear structure data maintained by the National Nuclear Data Center. Brookhaven National Laboratory. (2011). <http://www.nndc.bnl.gov/endl/>. Accessed 2011